European Polymer Journal 219 (2024) 113384

Contents lists available at ScienceDirect

European Polymer Journal

journal homepage: www.elsevier.com/locate/europolj

Bio-based ester- and ester-imine resins for digital light processing 3D printing: The role of the chemical structure on reprocessability and susceptibility to biodegradation under simulated industrial composting conditions

Anna Liguori [a,b,*], Naba Kumar Kalita [a], Grazyna Adamus [c], Marek Kowalczuk [c], Maria Letizia Focarete [b], Minna Hakkarainen [a,**]

[a] KTH Royal Institute of Technology, Department of Fibre and Polymer Technology, Teknikringen 58, 100 44 Stockholm, Sweden
[b] Department of Chemistry "Giacomo Ciamician", University of Bologna, 40126 Bologna, Italy
[c] Centre of Polymer and Carbon Materials, Polish Academy of Sciences, 34. M. C. Skłodowska St., 41-800 Zabrze, Poland

ARTICLE INFO

Keywords:
Bio-based thermosets
Recycling
Biodegradation
Composting
Digital light processing 3D printing
Dynamic covalent bonds

ABSTRACT

Four biobased ester and ester-imine photocurable resins were formulated and evaluated for printability by digital light processing 3D printing. The resin formulations consisted of methacrylated eugenol alone or in combination with methacrylated poly(hydroxybutyrate)-oligomers and/or methacrylated vanillin-derived Schiff-base monomers. It was not possible to print methacrylated eugenol alone into coherent thermosets, likely due to the lower reactivity of the allyl-double bond. However, in combination with the other building blocks methacrylated eugenol improved the printability, although some over-curing phenomena were registered especially for the resins composed of methacrylated eugenol and methacrylated poly(hydroxybutyrate)-derived oligomers. The three formulations that were successfully printed to coherent thermosets were further evaluated for their solvent resistance, thermal and mechanical properties, reprocessability and biodegradability under simulated industrial composting conditions. The reprocessing experiments documented the synergic effect of ester and imine dynamic covalent bonds in favoring the preservation of the elastic modulus of the thermosets; while an evidently higher deterioration of the mechanical properties was registered for the ester-thermosets. The biodegradation studies highlighted a clear correlation between the biodegradation rate and the chemical structure of the thermosets, with the aliphatic components and ester and imine bonds increasing the thermosets' susceptibility to the biodegradation under simulated industrial composting conditions.

1. Introduction

Thermosets are outstanding polymeric materials generally characterized by higher modulus and stress at break, chemical resistance and thermal stability compared with thermoplastics. Thermosets find a myriad of applications especially for the realization of long-lasting objects, such as pipelines, automotive parts, medical equipment, storage boxes, electrical components [1].

The superior properties of thermosets mainly derive from the presence of covalent crosslinks between the macromolecule chains, that lead to the formation of a network; differently from thermoplastics in which only secondary interactions exist between adjacent macromolecule chains. As a drawback, thermosets, including those derived from bio-based resources, do not fit the requirements of a circular economy [2,3] due to their limited recyclability, leading at best to downcycling or energy recovery. Recently, great efforts have been devoted to re-designing the chemical structure of thermosets by replacing some of the permanent covalent bonds with dynamic covalent linkages, such as imine and ester bonds, among others. This can, under correct conditions, enable reprocessing [4,5]. Imines have been demonstrated to show a great potential for the reformation of the network during the reprocessing. The metathesis pathway, consisting of exchange reactions

* Corresponding author at: KTH Royal Institute of Technology, Department of Fibre and Polymer Technology, Teknikringen 58, 100 44, Stockholm, Sweden.
** Corresponding author.
E-mail addresses: anna.liguori@unibo.it (A. Liguori), minna@kth.se (M. Hakkarainen).

https://doi.org/10.1016/j.eurpolymj.2024.113384
Received 9 June 2024; Received in revised form 4 August 2024; Accepted 10 August 2024
Available online 11 August 2024

between adjacent imine functions can be activated by temperature even in the absence of catalysts [6]. In this context, the possibility to induce Schiff-base reactions between bio-based molecules (i.e. vanillin [7–10], lignin [11]), syringaldehyde [12], soybean oil [13,14]) and a wide range of diamines and triamines has been reported for the synthesis of thermosets able to preserve their mechanical properties after the reprocessing [6]. The reprocessing of thermosets having dynamic ester bonds in their structure can generally occur in the presence of a transesterification agent and it mainly exploits the transesterification reaction between ester bonds and hydroxyl groups [15]. This pathway has been utilized for a wide range of epoxy resins [16–19], but also for the preparation of thermoplastic-derived thermosets, including networks obtained by modification of poly(lactic acid) [20], poly(butylene terephthalate) [21,22] and polyethylene [23].

However, for specific application and in cases where the number of reprocessing cycles leads to a drastic deterioration of the original properties, an additional waste management option is needed [24]. In this context, the biodegradation of polymers has been considered a valuable strategy, leading to products such as compost for agriculture in the case of composting, and biogas in the case of anaerobic digestion [25]. Among thermoplastics, polylactide, polycaprolactone, poly(3-hydroxybutyrate) (PHB), and their copolymers are the most studied aliphatic polyesters for a wide variety of applications, and thanks to their aliphatic structures with widely available ester bonds they are particularly suitable for biodegradation [26]. The degradation process can proceed according to different mechanisms, including chemical hydrolysis and microbial degradation, but ultimately the aerobic biodegradation, expected e.g. under industrial composting conditions, leads to the formation of CO_2, H_2O, and biomass. The degradation proceeds either from the surface or throughout the bulk and it is controlled by a wide variety of structural parameters, such as the morphology, chain orientation, chemical composition, stereochemical structure and molecular weight; but it also highly depends on the characteristics of the environment [26]. As an example, poly(L-lactide) was demonstrated to biodegrade in the presence of a mixed culture of compost microorganisms, while no important signals of degradation were registered in the corresponding abiotic medium. Moreover, a rapid decrease of molecular weight was observed in the biotic environment; while it was not detected in the abiotic environment [27]. Cellulose, as a biopolymer, is inherently biodegradable, but this process can be hindered by the chemical modifications performed to improve the processability and material properties, clearly demonstrating that structural characteristics, such as the type of modification and degree of substitution, are important factors controlling the degradation [28,29].

The biodegradation of thermosets has been hardly investigated, but it is expected to be more limited compared to linear counterparts. A few works have reported preliminary attempts to assess the potential of bio-based thermosets to be biodegraded in soil or in compost. As an example bio-based tannic acid epoxy resins cured in the presence of bio-based hardener poly(amido amine), and showing suitability as adhesives, were subjected to microbial biodegradation [30]. The SEM analysis documented erosion taking place on the surface of the thermosets after 4 weeks of incubation, mainly ascribable to the presence of hydrolysable esters and potentially cleavable amide linkages. Bio-based thermosets, derived from soybean oil, were subjected to soil-burial tests for 8 months; the results documented that the weight reduction during the test was affected by the thermoset's composition, crosslinking density and biodegradation time [31]. Methacrylated vanillyl alcohol was polymerized with acrylated epoxidized soybean oil for the obtainment of bio-based thermosets. The samples were buried in the garden soil for three months and a weight loss around 15 % was reached at the end of the test; however, no important alterations in the ATR-FTIR spectra were detected after the degradation test [32]. Biodegradation was also not confirmed by following CO_2 release.

It is envisioned that the structure of the thermosets, including the presence of aromatic or aromatic-aliphatic units and the presence of dynamic covalent bonds will influence both the reprocessability of the materials and their susceptibility to biodegradation, during e.g., composting. Therefore, we designed four distinct bio-based resins for digital light processing 3D printing (DLP), consisting of methacrylated eugenol alone and in combination with photocurable PHB-derived oligomers, or vanillin-derived Schiff-base monomers, or both. The structures of the thermosets were carefully designed in order to investigate the role of the ester and imine dynamic covalent bonds, as well as of the aliphatic and aromatic structures, on the reprocessability and biodegradability under simulated industrial composting conditions. Indeed, methacrylated eugenol is a short aromatic molecule showing ester functions in its structure; the PHB-derived oligomer is an aliphatic component with higher flexibility, higher density of ester groups and expected susceptibility to biodegradation; vanillin-based Schiff-base monomer is an aromatic-aliphatic molecule presenting imine functions in its structure. The printability, chemical and physical properties of the thermosets, as well as their reprocessability and biodegradability under simulated industrial composting conditions were also investigated and correlated with the structure and composition of the resins.

2. Materials and methods

2.1. Materials

The polyhydroxyalkanoate used in this study was poly(3-hydroxybutyrate) (PHB) produced by Tianan Biologic Material Co, China. The purity of this PHB was over 98 % and the content of 3-hydroxyvalerate units was below 2 % as revealed by ^{1}H NMR.

Vanillin (V) (99 %), ethylene carbonate (EC) (98 %), potassium carbonate (K_2CO_3) (≥99 %), *N,N*-dimethylformamide (DMF) (≥99 %), methacrylic anhydride (MAA) (94 %), ethylenediamine (ED) (≥99 %), eugenol (99 %), 1,4 butanediol (BDO) (99 %), phenylbis(2,4,6-trimethylbenzoyl)phosphine oxide (BAPO) (97 %) were purchased from Sigma-Aldrich. Magnesium sulfate (99 %), ethyl acetate (EtOAc) (≥99 %), dichloromethane (DCM) (≥99 %), n-heptane (≥99 %), acetone (≥99.5 %), deuterated chloroform (CDCl3) (99.8 atom % D) were purchased from VWR. Titanium (IV) butoxide (TBO) (≥97 %) and 4-(dimethylamino)pyridine (DMAP) (≥99 %) were purchased from Fluka, sodium bicarbonate (≥99 %) from Merck and sodium hydroxide (NaOH) (≥99 %) from Fisher Scientific. All chemicals and solvents were used as received.

2.2. Synthesis of methacrylated oligomeric PHB-diol (MOHB)

2 g of PHB and 3 mL of BDO were added to a 100 mL round-bottom flask and stirred at 190 °C for 15 min in N_2 atmosphere under reflux to melt the polymer. 8 mg of TBO, previously solubilized in toluene with a concentration of 0.01 mg/μL, was then added to the system and the reaction was carried out for additional 5 min [33]. Afterward, the mixture was poured in 20 mL of distilled water and kept under stirring at room conditions for 3 h. The white precipitate (PHB-diol) was collected through filtration and dried in the vacuum oven at 30 °C for 48 h.

The PHB-diol was subjected to a methacrylation reaction to obtain methacrylated PHB-diol (MOHB). 2 g of PHB-diol, 18 mL of MAA and 0.02 g of DMAP were added to a 100 mL round-bottom flask and kept under stirring at 60 °C for 24 h. The product of the reaction was then precipitated in 50 mL of n-heptane, filtered, solubilized in chloroform and again precipitated in heptane. The procedure was repeated three times. Afterwards, the collected MOHB monomer (white powder, reaction yield 20 %) was dried in vacuum oven at 30 °C for 48 h.

2.3. Synthesis of Schiff-base (SB) monomer and methacrylated eugenol

SB was produced following a three-step reaction, according to a previously reported procedure [7]. This included the synthesis of extended vanillin (Ext-V), its methacrylation (M−Ext−V) and the Schiff-

base reaction with ED. Briefly, 10 g of V, 6.38 g of EC, 11 g of K_2CO_3 and 100 mL of DMF were added to a 250 mL round bottom flask and kept under reflux in N_2 atmosphere at 110 °C for 12 h. The reaction mixture was then cooled down to room temperature, diluted with water (150 mL) and poured in EtOAc (150 mL). The aqueous phase was separated and extracted with EtOAc (2x100 mL). The organic phases were mixed, washed with water (2x200 mL), dried over magnesium sulfate, concentrated under reduced pressure and further dried in a vacuum oven at 60 °C for 12 h to recover Ext-V. The methacrylation of Ext-V was performed by mixing 10 g of ExtV, 8.58 g of MAA and 38 mg of DMAP in a 100 mL round-bottom flask. The reaction was carried out at 60 °C for 24 h under reflux. The resulting product was diluted with DCM (300 mL) and consequentially washed with saturated aqueous solution of sodium bicarbonate (2x300 mL), 0.5 M NaOH (2x300 mL), 1 M NaOH (2x300 mL) and distilled water (150 mL). The organic phase was dried over magnesium sulfate, concentrated at reduced pressure and dried under vacuum at 30 °C for two days. The resulting M−Ext−V was subjected to the Schiff-base reaction carried out by dissolving 12 g of M−Ext−V in 150 mL of DCM. After the complete solubilization, 1.37 g of ED was added and the reaction was performed at room temperature for 5 h. The mixture was washed and dried according to the procedure used for the methacrylation reaction, leading to SB monomer (pale yellow powder, reaction yield 70 %).

ME monomer (amber liquid, reaction yield 82 %) was obtained following a previously reported methacrylation reaction [34–36]. 30.00 g of eugenol, 30.99 g of MAA and 0.47 g of DMAP were mixed in a 250 mL round-bottom flask and kept at 45 °C in a N_2 atmosphere under reflux for 24 h. Afterwards, the mixture was subjected to the same washing and drying procedure described for M−Ext−V.

2.4. Resin composition and digital light processing (DLP) 3D printing

For the production of the thermosets, the synthesized monomers were combined to resins according to the compositions reported in Table 1 and dissolved in DCM with a concentration of 70 % w/v (g of resin/mL of DCM). BAPO with a concentration of 5 % w/w (g of BAPO/g of resin) was used as a photo-initiator. The resins were subjected to DLP 3D printing (Asiga MAX X27 UV) with a 385 nm light source. The exposure times and burn-in exposure times, determined by the software for each formulation, are reported in Table 1. The layer thickness and light intensity were set to 0.05 mm and 28.8 mW/cm^2, respectively, for each solution. No additional post-curing processes were performed on the printed thermosets. Thermosets were printed in form of rectangular bars (26.00 x 1.53 x 0.75 mm^3), films (31.71 x 19.77 x 0.75 mm^3) and "sun & moon" object (overall volume of 20.62 x 16.62 x 1.98 mm^3).

2.5. Reprocessing of thermosets

0.5 g of each thermoset was cut in small pieces with the help of a scissor, transferred to a 25 x 25 x 0.5 mm^3 square-shaped mold and hot-pressed at 120 °C, 2 MPa for 15 min. All the thermosets underwent two mechanical reprocessing cycles, both performed at the same conditions. Thermosets subjected to one mechanical reprocessing were labeled SB+ME_R1, MOHB+ME_R1 and SB+MOHB_R1. Thermosets subjected to two mechanical reprocessing cycles were labeled SB+ME_R2, MOHB+ME_R2 and SB+MOHB+ME_R2. No transesterification catalysts were used for the reprocessing

2.6. Biodegradation under simulated composting condition

The test samples were subjected to simulated industrial composting conditions according to previously reported procedure at 58 ± 2 ℃ up to 180 days [37]. The percentage of biodegradation was quantified by respirometry analysis. The set up with 1 L glass reagent bottles and 1 M KOH as CO_2 absorber was used for calculating the carbon mineralization. The amount of CO_2 released from the test samples was determined by titration and ASTM D5988 and D5338 were utilized to calculate the percentage mineralization using the following equation

$$\%Biodegradation = \frac{C_t - C_b}{C_{th}} \times 100 \quad (1)$$

where C_t is the amount in mg of gaseous-carbon produced; C_b is the amount in mg of carbon produced from blank and C_{th} is the amount in mg of carbon in the test compound. The weight percentage of carbon in each thermoset is reported in Table S1.

2.7. Characterizations

^{1}H NMR spectra of all the monomers was recorded by an Avance 400 (Bruker, U.S.A.) spectrometer (400 MHz), with 16 scans using $CDCl_3$ as the solvent and also as the internal standard for calibrating the chemical shift.

Size exclusion chromatography (SEC), with chloroform (2 % v/v toluene) as eluent, was utilized for molecular weight analysis of PHB and PHB-diol. It was performed with a Malvern GPCMAX instrument equipped with a refractive index (RI) detector and an autosampler, a PLgel 5 μm guard column (7.5 × 50 mm) and two PLgel 5 μm MIXED-D (300 × 7.5 mm) columns. The flow rate was 0.5 mL min^{-1} and the temperature was kept at 35 °C. Calibration was performed with polystyrene standards covering a molecular weight (M_p) range from approximately 400 to 400,000 g/mol.

A PerkinElmer Spectrum 2000 Fourier transform infrared (FTIR) spectrometer (Norwalk, CT) equipped with an attenuated total reflectance (ATR) sampling accessory was employed to characterize the chemical structures of the monomers and thermosets. All the spectra were recorded in the wavenumber range of 4000–600 cm^{-1} using 16 scans at a resolution of 4 cm^{-1}.

Gel content measurements were carried out to investigate the degree of curing and solvent resistance of the thermosets by immersing each thermoset (around 10 mg) in 2 mL solvent for 72 h; three common solvents (DCM, EtOH and acetone) were investigated for the test. After being removed from the solvent, the samples were dried in vacuum oven at 60 °C until a constant weight was reached. The gel fraction for each sample was determined according to equation (1).

$$Gel\ content = \frac{m_f}{m_i} x100 \quad (3)$$

where m_f is the final weight of the sample after 72 h of immersion and drying; while m_i is the initial weight of each sample before the immersion. The analysis was performed in triplicate for each sample and for each solvent.

Thermogravimetric analysis (TGA) of the thermosets and monomers

Table 1
Abbreviations, compositions and printing parameters of the printed thermosets.

Thermoset abbreviations	ME monomer [w/w$_{tot}$ %]	SB monomer [w/w$_{tot}$ %]	MOHB monomer [w/w$_{tot}$ %]	Exposure time for each layer [s]	Burn-in exposure time [s]
ME	100	–	–	60	172
SB+ME	50	50	–	108	164
MOHB+ME	83	–	17	45	101
SB+MOHB+ME	41.5	41.5	17	87	152

was performed by a TGA/SDTA851e (METTLER TOLEDO, U.S.A.). Samples with a weight around 5 mg were inserted in 70 μL ceramic crucibles and subjected to a heating scan from 30 °C to 600 °C with a heating rate of 10 °C/min and under a 50 mL/min nitrogen flow. Differential scanning calorimetry (DSC) analysis of the thermosets was performed on a METTLER TOLEDO DSC820. Samples with a weight around 5 mg were sealed into 100 μL aluminum crucibles. All the samples were first cooled to −10 °C and then subjected to a heating ramp (10 °C/min) up to 160 °C, under a nitrogen flow rate of 50 mL/min. DSC was calibrated with indium calibration standard.

3D printed bars and reprocessed thermosets were subjected to stress–strain measurements performed by using an Instron 5944 equipped with a 500 N load cell. Samples were conditioned in a controlled environment with a temperature of 22 °C and 50 % relative humidity for 2 days before testing.

3. Results and discussion

Polyester and polyester-imine thermosets were obtained by DLP 3D printing of the synthesized photocurable resins, derived from the combination of methacrylated biobased monomers and oligomers, as shown in Fig. 1a and 1b. The printed thermosets were evaluated for their chemical and physical properties, reprocessability and biodegradation potential under simulated industrial composting conditions.

3.1. DLP 3D printing of the resins

The chemical structures of the resin components ME and SB were first confirmed by ^{1}H NMR analysis (Figures S1 and S2), which documented the successful methacrylation of eugenol and the triple step reaction to synthesize SB starting from vanillin [6,34]. Due to the high molecular weight (above the upper range of calibration curve, 400 000 g/mol), PHB was as a first step subjected to a transesterification reaction with a diol (BDO) in order to obtain PHB oligomers with two terminal –OH functions for further methacrylation. The transesterification, performed in the absence of any solvent according to the procedure reported in the Experimental Section, led to the formation of oligomers with a Mw around 1400 g/mol (Figure S3) with incorporated aliphatic BDO segment in their structure (Figure S4). Moreover, the absence of significant peaks at 5.8 ppm, ascribed to crotonate vinylic proton signal [38], demonstrates that the applied reaction conditions prevented the occurrence of undesired thermal degradation phenomena [33]. The ATR-FTIR analysis in Figure S6 confirms the presence of –OH terminal functions in PHB-diol (band at 3619–3030 cm^{-1}). In tune ^{1}H NMR spectroscopy (Figure S5), documents the consumption of these groups during the methacrylation step together with the appearance of a new peak at 1640–1650 cm^{-1}, supporting the introduction of the vinyl groups [39].

ME functions as a reactive diluent as it is able to partially solubilize both resins. Due to the presence of vinyl groups it will be incorporated in the thermoset structures. However, the complete dissolution of SB and MOHB was not reached and the use of a solvent turned out to be unavoidable for the preparation and DLP printing of the employed formulations. However, the partial solubilization of the solid resins in ME reduced the required volume of DCM in particular in presence of MOHB. In order to have more relevant comparison among the thermosets in

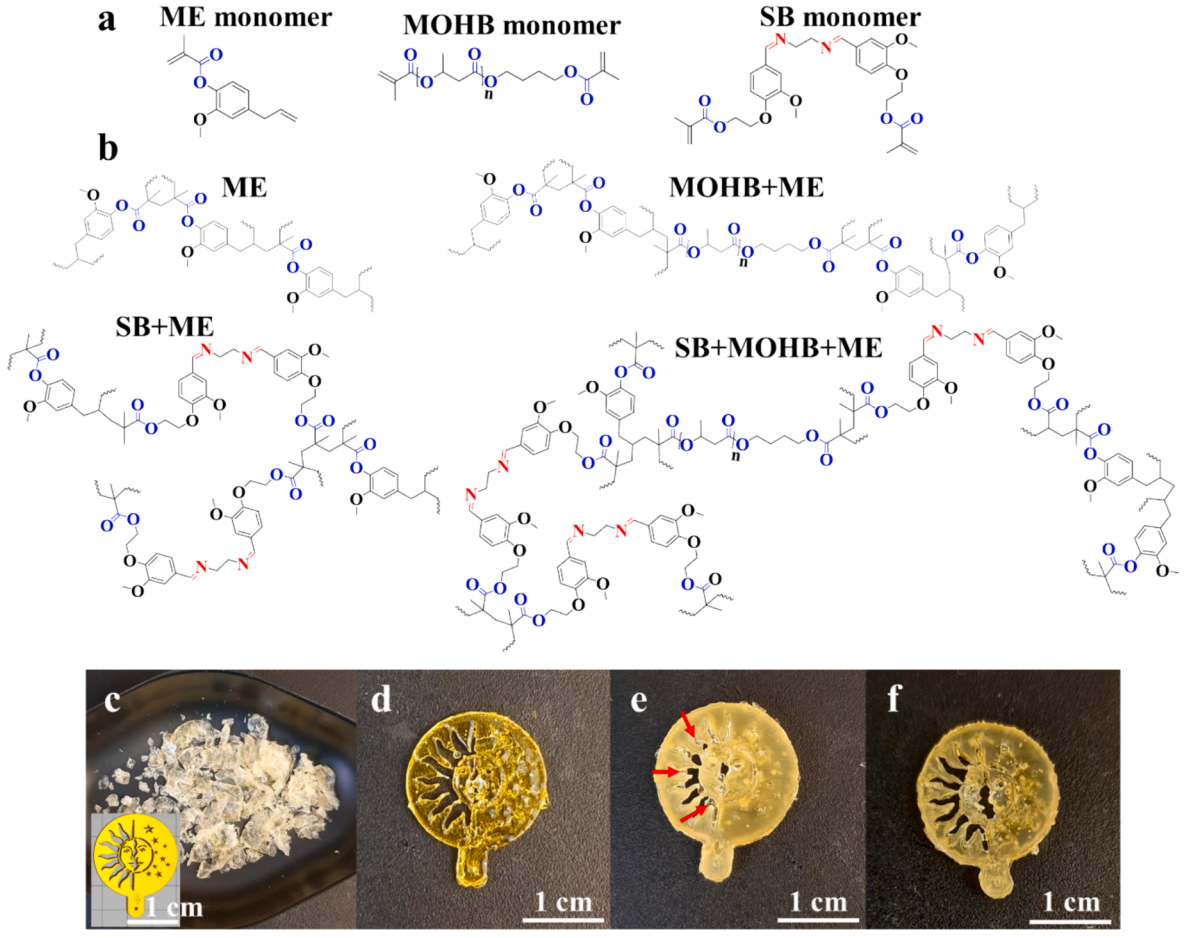

Fig. 1. (a) Chemical structures of monomers and (b) schematic chemical structures of the cured thermosets. Digital light processing 3D printed "sun & moon" objects printed with: (c) ME; (d) SB+ME; (e) MOHB+ME and (f) SB+MOHB+ME resins. Inset of (c): computer-aided design model of the "sun & moon" model.

terms of printing conditions and resulting properties, DCM was also employed during printing of ME. The printability of the resins as well as the layer exposure times strongly correlated with the chemical structure and composition of the resins (Fig. 1b). ME has only one methacrylate group per molecule and in addition a less reactive allyl group, which likely prevented its curing to a coherent thermoset [40]. The introduction of dimethacrylated components in the formulation, i.e. MOHB, SB or both, significantly improved the printability, enabling the fabrication of thermosets showing acceptable printing fidelity, especially in the case of SB+ME resins, as documented in Fig. 1 c-f.

The analysis of exposure times needed for the layer-by-layer photopolymerization of SB+ME, MOHB+ME and SB+MOHB+ME resins clearly highlights an increase of this parameter with the higher content of aromatic rings and imine-groups in the resin formulation. This suggests that both the aromatic rings and the imine-groups act has light absorbing agents, favoring the capture of the UV radiation and preventing its penetration towards undesired layers. It was somewhat unexpected, that the longest exposure time was needed for the curing of SB+ME, since the relatively high M_w of MOHB could have led to lower reactivity for this monomer with respect to SB. The explanation to the observed phenomenon lies in the potential of aromatic and Schiff-base functions to contribute to light absorption, at the same time preventing the propagation of the radiation towards undesired layers of the resin [41–43]. In agreement with this consideration, the presence of SB in the resin formulation reduced the over-curing clearly present in MOHB+ME as highlighted by the arrows in Fig. 1e.

3.2. Characterization of the thermosets

The ATR-FTIR analysis, reported in Fig. 2a, documents the presence of ester functions in all the thermosets, although a slight shift towards higher wavenumbers is registered for ME. Moreover, a peak at 1804 cm^{-1} undetected in ME monomer (Figure S7) can be observed in ME and it might be ascribed to the occurrence of side reactions on the allyl functions of eugenol during the photopolymerization. The presence of this peak, although with a significantly lower intensity is also detected in MOHB+ME, which turns out to show a spectrum quite similar to ME, except for the presence of the ester peak at 1731 cm^{-1} instead of 1736 cm^{-1}, in tune with the composition of the resin. SB+ME as well as the tricomponent thermoset do not show any peak at 1804 cm^{-1} due to the lower content of ME in the resins, clearly confirming the incorporation of SB in the networks. The peak at 1640 cm^{-1}, detected in SB monomer (Figure S8) and in both the SB containing thermosets, confirm the presence of imine functions [7,8], nonetheless its overlapping with the stretching vibration of C=C. In this frame, it is possible to notice that this peak at 1640 cm^{-1} appears very clear in ME monomer (Figure S7), while it has low intensities in all the thermosets, confirming the occurred photopolymerization [44,45].

Gel content measurements were not performed on ME due to the small size of the fragments obtained after the DLP. For the other thermosets the gel content results reported in Fig. 2b documented rather similar properties in acetone. SB+ME and SB+MOHB+ME show a comparable solvent resistance in DCM and EtOH; while, MOHB+ME presents the lowest gel content values in these two solvents. Typically, post-curing is utilized after DLP to complete the curing process. Here, no post-curing treatment was performed in order to investigate the properties of as-printed materials, which likely explains the low gel content values (56–76 %) of all three thermosets in DCM. This conclusion is supported by our previous study investigating the influence of post-curing on properties of DLP printed SB thermosets (without ME),

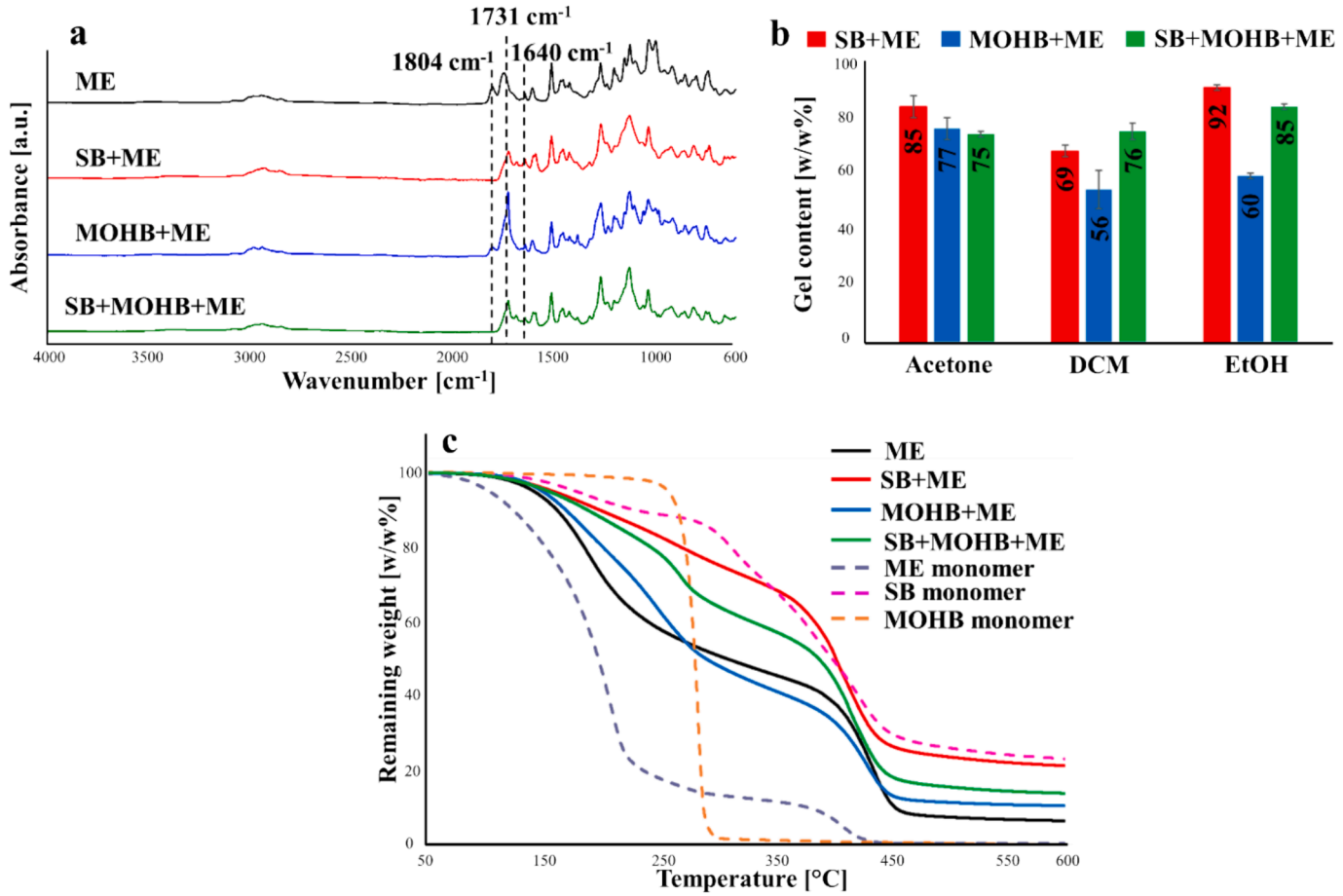

Fig. 2. (a) ATR-FTIR spectra and (b) gel content measurements of all the thermosets. (c) TGA curves of all the thermosets and monomers.

where it was shown that UV post-curing of the printed thermosets increased the gel content from 67 to 87 %, i.e. before post-curing the gel content of SB thermoset (67 %) was similar to gel content of SB+ME here (69 %) [46].

In addition, previous studies showed the low reactivity of the allyl function in ME monomers during UV-initiated radical reaction leading to formation of a defective networks and low gel contents [35,36]. The inferior solvent resistant properties of MOHB+ME with respect to the other thermosets can be ascribed to the presence of this allyl functions as well as to the lower density of vinyl groups also due to the relatively high molecular weight of MOHB, leading to lower crosslink density.

The thermal stability of the thermosets and of their building blocks was investigated by means of TGA. As observable in Fig. 2c and in Table 2, all the thermosets show an onset of degradation ($T_{deg1\%}$ and $T_{deg2\%}$) around 110–127 °C. The $T_{deg5\%}$ is reached at 145 °C in the case of ME and MOHB+ME while the SB containing thermosets reached the $T_{deg5\%}$ at around 155 °C. From the comparison of ME and ME monomer thermal degradation curves, it is possible to observe that ME is more thermally stable than its respective monomer, in tune with the occurrence of the photopolymerization. The two degradation steps registered for ME at around 178 °C (T_{Ideg}) and 433 °C (T_{IIdeg}) are ascribed to the decomposition of dangling chains and to the random scission of crosslinked chains, respectively [36,47,48].

In agreement with its higher molecular weight, MOHB is characterized by good thermal stability, preserving almost completely its initial weight up to 250 °C. The 17 % w/w concentration of MOHB in MOHB+ME thermoset is however not enough to move the onset of degradation towards higher temperatures. However, the transition of T_{Ideg} from 178 °C for ME to 192 °C MOHB+ME is registered, suggesting an increase of the thermal stability of the thermoset in the presence of MOHB. Interestingly, the presence of ME monomer in SB+ME resin leads to thermosets characterized by significantly lower thermal stability than the previously reported SB thermosets [7] and SB monomer. In agreement with the previous considerations, this result can be explained considering the uncompleted photopolymerization of ME monomer in the network and the presence of branched segments from which the thermal decomposition can start. SB+MOHB+ME shows a decomposition curve very similar to the one of ME, but there is a shift towards higher percentage of residual weights, in tune with the presence of SB and MOHB in the network. According to the DSC characterization (Table 2 and Figure S9), all the thermosets show T_g around 60–70 °C.

3.3. Reprocessing of the thermosets

In the framework of reprocessing of prepared ester thermosets, the most exploited pathway relays on the induction of ester-hydroxyl exchange reactions [15]. This pathway, also known as dynamic transesterification reaction (DTER), has been widely reported in literature mainly for the mechanical recycling of epoxy thermosets [49,50]. This is enabled by the contextual presence of ester functions and free OH groups in the network, often in the presence of a catalyst to accelerate the reconstruction of the crosslinked network [51–53]. In our thermosets, due to the absence of available terminal hydroxyl groups, the reprocessing could possibly proceed accordingly with a different associative pathway of the ester functions called esterolysis. The esterolysis is an ester-ester exchange mechanism taking place when two carbonyls of adjacent ester bonds experience formation of an association complex and the acyl groups of the original esters are switched. This pathway has been demonstrated to take place in thermoplastic polyesters [54] and it has been recently exploited for the development of crosslinked network starting from linear polyesters in the presence of a catalyst [55,56].

In our study, the DLP 3D printed thermosets were cut in small pieces and hot-pressed in the absence of a catalyst at 120 °C, 2 MPa for 15 min. These mild conditions did not induce any important weight loss in the thermoset as the weight of the reprocessed sample was comparable to the amount of grinded original thermoset used for the process. Moreover, these conditions promoted activation of the metathesis pathway, an associative pathway of the imine bonds [6], in SB-containing thermosets and the results also indicate activation of ester-ester exchange pathway in all the thermosets. Due to the unsuccessful recovery of coherent thermosets, ME was not considered for the reprocessing. As observable in Fig. 3a and 3b, all the thermosets show good homogeneity after one or two reprocessing cycles.

The comparison of the mechanical properties in Fig. 3c and Table 3 shows that the DLP 3D printed SB+MB thermoset has the highest elastic modulus, strain and stress at break, while the lowest elastic modulus, strain and stress at break is registered for MOHB+ME. Intermediate values are measured for the thermoset containing both SB and MOHB.

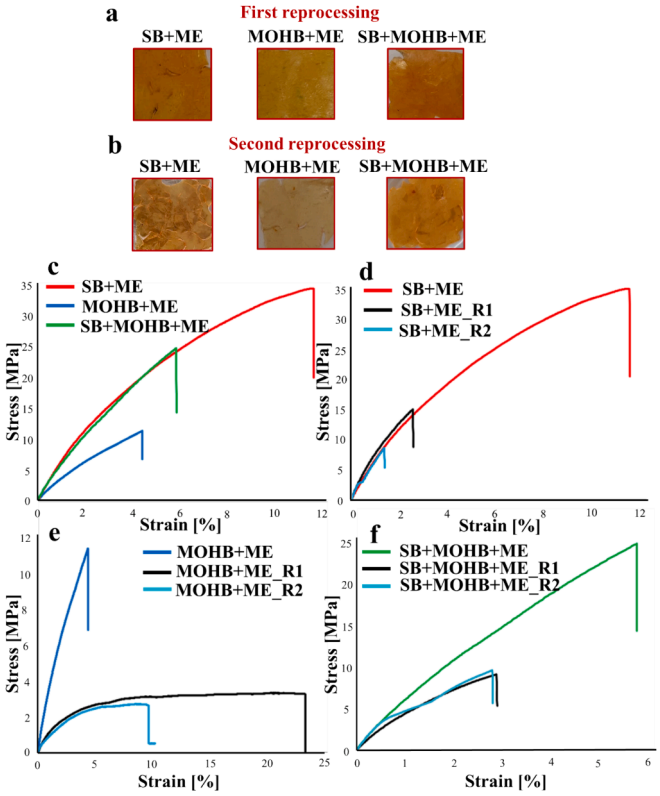

Fig. 3. Pictures of SB+ME, MOHB+ME and SB+MOHB+ME after (a) the first and (b) the second reprocessing cycle. Stress–strain curves of (c) DLP 3D printed SB+ME, MOHB+ME, SB+MOHB+ME; and DLP 3D printed and thermally once (R1) or twice (R2) reprocessed samples (d) SB+ME, SB+ME_R1, SB+ME_R2; (e) MOHB+ME, MOHB+ME_R1, MOHB+ME_R2; (f) SB+MOHB+ME, SB+MOHB+ME_R1, SB+MOHB+ME_R2.

Table 2
Thermal properties of all the thermosets.

Sample	T_g [°C]	$T_{deg1\%}$ [°C]	$T_{deg2\%}$ [°C]	$T_{deg5\%}$ [°C]	T_{Ideg} [°C]	T_{IIdeg} [°C]	Residue [w/w%]
ME	68 ± 7	110 ± 5	112 ± 5	143 ± 5	178 ± 10	433 ± 3	8 ± 3
SB+ME	63 ± 5	109 ± 1	127 ± 1	157 ± 3	–	405 ± 1	18 ± 4
MOHB+ME	66 ± 1	115 ± 4	127 ± 3	147 ± 3	192 ± 7	429 ± 1	11 ± 4
SB+MOHB+ME	70 ± 4	109 ± 1	126 ± 1	154 ± 2	269 ± 1	419 ± 3	17 ± 5

Table 3
Mechanical properties of DLP 3D printed thermosets and the thermosets after one or two thermal reprocessing cycles.

Sample	Stress [MPa][a]	Strain [%][a]	E [MPa] [a]
SB+ME	32 ± 5	11 ± 1	619 ± 157
SB+ME_R1	10 ± 4	2 ± 1	677 ± 91
SB+ME_R2	9 ± 4	3 ± 2	766 ± 105
MOHB+ME	9 ± 1	4 ± 1	424 ± 56
MOHB+ME_R1	2 ± 1	17 ± 6	136 ± 52
MOHB+ME_R2	3 ± 1	10 ± 1	56 ± 28
SB+MOHB+ME	27 ± 3	7 ± 2	636 ± 184
SB+MOHB+ME_R1	7 ± 1	2 ± 1	458 ± 63
SB+MOHB+ME_R2	7 ± 3	2 ± 1	431 ± 140

[a] The measurements were performed on 4 specimens for each sample.

This can be explained by the higher aliphatic content and expected lowed degree of crosslinking due to the relatively high molecular weight of MOHB. In comparison, the elastic modulus of DLP 3D printed SB thermoset in our previous study was 1207 MPa, i.e. twice the value reported for SB+ME (619 MPa) in current study. The relatively low elastic moduli registered for all the thermosets could thereby be explained by the high content of ME monomer with less reactive allyl-groups.

When comparing the mechanical properties before and after reprocessing, in Fig. 3d-f and Table 3, the different processing methods should be noted. The original samples were DLP 3D printed and the reprocessing took place by hot pressing. Therefore, direct comparison of the mechanical properties of original and reprocessed samples should be made with care. While relatively large differences were observed between the DLP printed and once thermally reprocessed samples, the mechanical properties of once and twice reprocessed samples were almost identical to each other in the case of SB containing thermosets, SB+ME (Fig. 3d) and SB+MOHB+ME (Fig. 3f). Table 3 shows that the differences are smaller than the standard deviations. In contrary, the reprocessability of the thermoset MOHB+ME without SB and dynamic imine-groups was not as good. Although it could be reprocessed twice to coherent thermosets, a significant reduction in elastic modulus and strain at break was observed after second reprocessing (Fig. 3e). This correlates with the fact that transesterification catalysts are typically required for thermal reprocessing of ester thermosets, while imine metathesis can be activated in the absence of catalysts by moderate temperatures [57]. In addition, some thermal degradation of MOHB segments resulting in the formation dangling chains with crotonate end groups could take place during the thermal reprocessing [58,59]. This would additionally lower the crosslinking degree leading to reduction in elastic modulus, while strain at break could first increase and then decrease at higher degree of degradation.

Last, several structural changes might contribute to the relatively large differences in the mechanical properties of DLP printed and once thermally reprocessed thermosets. The analysis of the chemical structure of the reprocessed thermosets, reported in Fig. 4, further documents an increase of the intensity of the peak at 1684 cm^{-1} for SB+ME_R1 and SB+ME_R2 with respect to the original samples, suggesting that the decrease of the stress and strain at break after the reprocessing could be due to the opening of some iminebonds. Moreover, a decrease of the intensity of the peak at 950 cm^{-1}, ascribable to the C=C of SB [7], with respect to the adjacent peak at 913 cm^{-1} can be detected and it advocates a possible completion of the curing during the hot-press. In earlier work, it was shown that completion of curing of DLP printed SB thermosets by UV-light led to retained or slightly increased elastic modulus and stress at break and decreased strain at break [46].

The spectra of MOHB+ME_R1 and MOHB+ME_R2 show broadening of the ester peak with appearance of a shoulder, that likely indicates chain scissions due to thermal degradation leading to formation of free carboxyl-groups. Moreover, a reduction of the intensity of the peak at 1230 cm^{-1} is observed with the reprocessing. This signal was assigned to the conformational band of the helical segments of PHB-derived

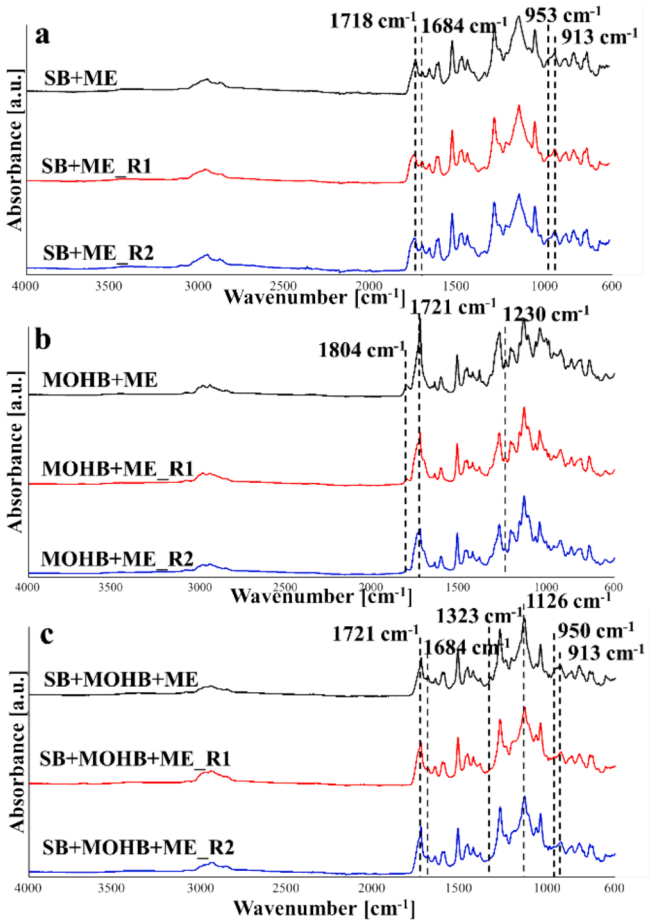

Fig. 4. ATR-FTIR spectra of (a) SB+ME as printed and after the first and second reprocessing cycle; (b) MOHB+ME as printed and after the first and the second reprocessing cycle; (c) SB+MOHB+ME as printed and after the first and the second reprocessing cycle.

segments [60,61]; its reduction suggests a modification of their conformation in the network. The ATR-FTIR analysis of the reprocessed tri-component thermosets highlights a very slight increase of intensity of the peak at 1684 cm^{-1} and the disappearance of the signal at 1230 cm^{-1}, ascribable to SB and MOHB components, respectively. Moreover, similar to reprocessed SB+ME, a decrease of the intensity of the peak at 950 cm^{-1} was registered also for this thermoset, documenting the completion of the curing during the hot-press. Interestingly for all the thermosets, no differences were noticed between the spectra obtained after the first and the second reprocessing cycle.

3.4. Biodegradation under simulated industrial composting conditions

The characterization of the thermosets clearly highlights the influence of the chemical structure on resulting properties and reprocessing. It has been already demonstrated that the efficiency in biodegradation of thermoplastics is very sensitive to the polymer structure, making the structure-biodegradation relationship often difficult to be completely predicted [24]. In order to investigate the effects of the thermosets' structure on the biodegradation under simulated industrial composting conditions, a six-month test cycle was performed on all the thermosets.

The results of the CO_2 measurements over 180 days under simulated industrial composting conditions, depicted in Fig. 5, reveal a clear correlation between the biodegradation rate and the chemical structure of the thermosets. The presence of aromatic structures in ME and SB+ME initially hinders their degradation, with the lag phase persisting for over two months and the final degree of biodegradation reaching only around

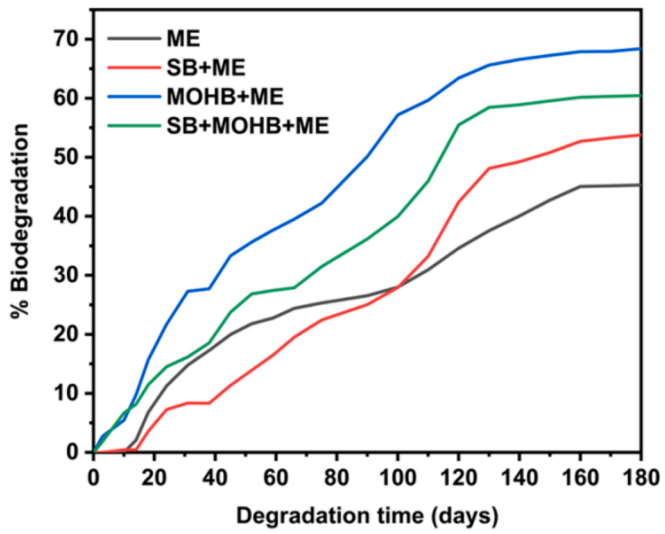

Fig. 5. Thermosets' biodegradation rate under simulated industrial composting conditions.

45–50 % after 180 days. Conversely, the inclusion of the aliphatic MOHB units, even at a low content of 17 w/w%, enhances the compostability of the tri-component thermoset. This formulation surpasses the lag phase after 40 days and achieves a degree of biodegradation ~ 60 % at the end of the test. Notably, the MOHB+ME thermoset exhibits the most promising biodegradation outcome, with rapid kinetics overcoming the lag phase after 20 days and reaching a 65 % biodegradation rate within 180 days.

As widely documented, the degradation of polyesters is generally associated to a combination of abiotic and biotic mechanisms, i.e. chemical hydrolysis and microbial degradation. When the abiotic mechanism is dominant, a lag phase is generally observed. This phenomenon is assumed to correlate with the acclimatization of the microbial population to the environment and it is generally due to the presence of an exogenous material such as synthetic polymers that are not readily assimilable by microorganisms [62]. In tune with the previous considerations, the results suggest that the high density of aromatic rings makes ME and SB+ME less prone to the microbial attack with respect to the other samples showing aliphatic segments in their structures.

Despite showing the same MOHB content, MOHB+ME exhibits a somewhat faster biodegradation rate compared to the tri-component thermoset, which closely resembles SB+ME but with a shift toward higher degradation rates. The results can be ascribed to the higher crosslinking degree of the tri-component resin, confirmed by the gel-content measurements and mechanical analysis, which could make this thermoset less susceptible to biodegradation in comparison with MOHB+ME. The trends of the curves obtained for ME and SB+ME can be explained by considering two aspects. The low reactivity of the allyl-group of the ME monomer led to a non-coherent thermoset scarcely crosslinked and, therefore, characterized by a faster biodegradation kinetic than SB+ME as observable from day 0 to day 100. For longer testing time, the inversion of the trend of the two curves is ascribable to the synergic action of ester and imine bonds, which could accelerate the biodegradation kinetics. Indeed, similar to ester functions, the imine bonds can be hydrolysed and the imine-hydrolysis could also be catalysed by enzymes [63], favouring the breaking up of the crosslinked thermoset into branched polymeric and oligomeric structures.

4. Conclusions

The influence of the resin composition on the 3D printability as well as on the chemical and physical properties, reprocessability and biodegradability of the printed biobased thermosets was demonstrated. Due to the less reactive allyl-bond, the ME monomer was not photocurable alone into coherent thermosets. However, it had beneficial influence on the printability of resulting thermosets in combination with an aliphatic or aliphatic–aromatic component, such as MOHB or SB. The aromatic rings and Schiff-base linkages, both present in SB, can act as light absorbing agents in the resins reducing overcuring, as confirmed by the longer exposure times set up by the DLP software for the photopolymerization of both SB+ME and SB+MOHB+ME. The addition of MOHB or SB or both also improved the thermal stability of the thermosets, which can be explained by the increased degree of curing during. MOHB+ME thermoset demonstrated the lowest solvent resistance properties and mechanical properties in tune with lower crosslink density due to the relatively high molecular weight of MOHB.

All the thermosets were reprocessed twice through a hot-press procedure performed under relatively mild conditions and in the absence of a transesterification agent. The lower curing, degree of MOHB+ME together with the absence of imine linkages caused a drastic decrease of the mechanical properties of the reprocessed samples with respect to the original ones while the contextual presence of ester bonds and imine functions in SB+ME and SB+MOHB+ME enabled to larger extent the preservation of the elastic modulus with respect to the original samples and no significant alterations of the properties between the thermosets subject to one or two reprocessing cycles were observed.

The biodegradation studies documented reasonable susceptibility to biodegradation under industrial composting conditions. Although 90 % biodegradation required by composting standards was not reached in 180 days, the thermoset with highest biodegradation rate (MOHB+ME) reached almost 70 % biodegradation. The biodegradation rates clearly correlated with the chemical structure of the thermosets. Indeed, as expected, slower biodegradation kinetics were registered in presence of high content of aromatic structures and higher degrees of crosslinking, while the introduction of ester-based aliphatic components and the synergic action of ester and imine bonds increased the thermosets susceptibility towards biodegradation. In conclusion, we demonstrated the possibility to tune the chemical structure of the photopolymerized thermosets to enable repeated mechanical recyclability and/or susceptibility to biodegradation at the end of their useful life. The introduction of polyester-derived aliphatic component together with the contextual presence of ester and imine bonds in the thermoset structure pave the way to the design of next generation thermosets, which can be mechanically recycled or biodegraded at the end of their useful life.

Funding

The work was carried out in the frame of the project "Sustainable–Library of inedited bio-based multicomponent resins for the 3D-printing of self-healing, recyclable thermosets". The project has received funding from the European Union's Horizon 2020 research and innovation programme under the Marie Sklodowska-Curie grant agreement No 101021859 (A.L.) and Wenner-Gren Foundation, Grant No. UPD2021-0016 (N.K.K. and M.H.).

CRediT authorship contribution statement

Anna Liguori: Writing – original draft, Visualization, Validation, Methodology, Investigation, Funding acquisition, Formal analysis, Data curation, Conceptualization. **Naba Kumar Kalita:** Writing – review & editing, Visualization, Investigation, Formal analysis, Data curation. **Grazyna Adamus:** Writing – review & editing, Investigation. **Marek Kowalczuk:** Writing – review & editing, Investigation. **Maria Letizia Focarete:** Writing – review & editing, Validation. **Minna Hakkarainen:** Writing – review & editing, Validation, Supervision, Resources, Methodology, Funding acquisition, Conceptualization.

Declaration of competing interest

The authors declare that they have no known competing financial interests or personal relationships that could have appeared to influence the work reported in this paper.

Data availability

Data will be made available on request.

Additional data are available in the supplementary material of this article or from the corresponding author upon reasonable request.

Appendix A. Supplementary material

Supplementary data to this article can be found online at https://doi.org/10.1016/j.eurpolymj.2024.113384.

References

[1] Thermosets: Structure, properties and applications, Elsevier Recent Advances and Applications of Thermoset Resins, Second Edition, Edited by Qipeng Guo, Elsevier 2018.

[2] K. Van Doorsselaer. Chapter 12 - The role of ecodesign in the circular economy, CIES, Volume 1: Management and Policy (2022) 189-205. Doi: 10.1016/B978-0-12-819817-9.00018-1.

[3] M. Shamsuyeva, H.-J. Endres. Plastics in the context of the circular economy and sustainable plastics recycling: Comprehensive review on research development, standardization and market, Compos., Part C: Open Access 6 (2021) 100168. [Doi: 10.1016/j.jcomc.2021.100168.

[4] W. Zou, J. Dong, Y. Luo, Q. Zhao, T. Xie, Dynamic covalent polymer networks: from old chemistry to modern day innovations, Adv. Mater. 29 (2017) 14, https://doi.org/10.1002/adma.201606100.

[5] A. Durand-Silva, R.A. Smaldone, Recycling the unrecyclable with dynamic covalent chemistry, ACS Cent. Sci. 6 (2020) 836–838, https://doi.org/10.1021/acscentsci.0c00488.

[6] A. Liguori, M. Hakkarainen, Designed from biobased materials for recycling: imine-based covalent adaptable networks, Macromol. Rapid Commun. 43 (2022) 2100816, https://doi.org/10.1002/marc.202100816.

[7] A. Liguori, S. Subramaniyan, J.G. Yao, M. Hakkarainen, Photocurable extended vanillin-based resin for mechanically and chemically recyclable, self-healable and digital light processing 3D printable thermosets, Eur. Polym. J. 178 (2022) 111489, https://doi.org/10.1016/j.eurpolymj.2022.111489.

[8] Y. Xu, K. Odelius, M. Hakkarainen, Photocurable, thermally reprocessable, and chemically recyclable vanillin-based imine thermosets, ACS Sustainable Chem. Eng. 8 (2020) 17272–17279, https://doi.org/10.1021/acssuschemeng.0c06248.

[9] Y. Sun, D. Sheng, H. Wu, X. Tian, H. Xie, B. Shi, X. Liu, T. Yang, Bio-based vitrimer-like polyurethane based on dynamic imine bond with high-strength, reprocessability, rapid-degradability and antibacterial ability, Polymer 233 (2021) 124208, https://doi.org/10.1016/j.polymer.2021.124208.

[10] S. Wang, S. Ma, C. Xu, Y. Liu, J. Dai, Z. Wang, X. Liu, J. Chen, X. Shen, J. Wei, J. Zhu, Vanillin-derived high-performance flame retardant epoxy resins: facile synthesis and properties, Macromolecules 50 (2017) 1892, https://doi.org/10.1021/acs.macromol.7b00097.

[11] Z. Sun, B. Fridrich, A. De Santi, S. Elangovan, K. Barta, Bright side of lignin depolymerization: toward new platform chemicals, Chem. Rev. 118 (2018) 614, https://doi.org/10.1021/acs.chemrev.7b00588.

[12] H. Nabipour, X. Wang, L. Song, Y. Hu, A high performance fully bio-based epoxy thermoset from a syringaldehyde-derived epoxy monomer cured by furan-derived amine, Green Chem. 23 (2021) 501, https://doi.org/10.1039/D0GC03451G.

[13] F. Zhao, W.Q. Lian, Y.D. Li, Y. Weng, J.B. Zeng, Synthesis of epoxidized soybean oil-derived covalent adaptable networks through melt Schiff base condensation, Ind. Crop. Prod. 187 (2022) 115499, https://doi.org/10.1016/j.indcrop.2022.115499.

[14] X.L. Zhao, Y.Y. Liu, Y. Weng, Y.D. Li, J.B. Zeng, sustainable epoxy vitrimers from epoxidized soybean oil and vanillin, ACS Sustain. Chem. Eng. 8 (39) (2020) 15020–15029, https://doi.org/10.1021/acssuschemeng.0c05727.

[15] T. Liu, B. Zhao, J. Zhang, Recent development of repairable, malleable and recyclable thermosetting polymers through dynamic transesterification, Polymer 194 (2020) 122393, https://doi.org/10.1016/j.polymer.2020.122392.

[16] D. Montarnal, F. Tournilhac, M. Hidalgo, L. Leibler, Epoxy-based networks combining chemical and supramolecular hydrogen-bonding crosslinks, J. Polym. Sci., Part a: Polym. Chem. 48 (2010) 1133–1141, https://doi.org/10.1002/pola.23870.

[17] M. Capelot, D. Montarnal, F. Tournilhac, L. Leibler, Metal-catalyzed transesterification for healing and assembling of thermosets, J. Am. Chem. Soc. 134 (2012) 7664–7667, https://doi.org/10.1021/ja302894k.

[18] J. Han, T. Liu, S. Zhang, C. Hao, J. Xin, B. Guo, J. Zhang, Hyperbranched polymer assisted curing and repairing of an epoxy coating, Ind. Eng. Chem. Res. 58 (2019) 6466–6475, https://doi.org/10.1021/acs.iecr.9b00800.

[19] Y. Li, T. Liu, S. Zhang, L. Shao, M. Fei, H. Yu, Catalyst-free vitrimer elastomers based on a dimer acid: robust mechanical performance, adaptability and hydrothermal recyclability, Green Chem. 22 (2020) 870–881, https://doi.org/10.1039/C9GC04080C.

[20] J.P. Brutman, P.A. Delgado, M.A. Hillmyer, Polylactide vitrimers, ACS Macro Lett. 3 (2014) 607–610, https://doi.org/10.1021/mz500269w.

[21] Y. Zhou, J.G.P. Goossens, R.P. Sijbesma, J.P.A. Heuts, Poly(butylene terephthalate)/glycerol-based vitrimers via solid-state polymerization, Macromolecules 50 (2017) 6742–6751, https://doi.org/10.1021/acs.macromol.7b01142.

[22] A. Demongeot, R. Groote, H. Goossens, T. Hoeks, F. Tournilhac, L. Leibler, Cross-linking of poly(butylene terephthalate) by reactive extrusion using zn(II) epoxy-vitrimer chemistry, Macromolecules 50 (2017) 6117–6127, https://doi.org/10.1021/acs.macromol.7b01141.

[23] J. Ji, X. Liu, C. Lin, Y. Zhou, L. Dong, S. Xu, D. Sheng, Y. Yang, Reprocessable and recyclable crosslinked polyethylene with triple shape memory effect, Macromol. Mater. Eng. 304 (2019) 1800528, https://doi.org/10.1002/mame.201800528.

[24] N.K. Kalita, M. Hakkarainen, Integrating biodegradable polyesters in a circular economy, Curr. Opin. Green Sust. 40 (2023) 100751, https://doi.org/10.1016/j.cogsc.2022.100751.

[25] A. Morinval, L. Averous, Systems based on biobased thermoplastics: from bioresources to biodegradable packaging applications, Polym. Rev. 62 (2022) 4, https://doi.org/10.1080/15583724.2021.2012802.

[26] M. Hakkarainen, Aliphatic polyesters: abiotic and biotic degradation and degradation products, Adv. Polym. Sci. 157 (2002) 113–138, https://doi.org/10.1007/3-540-45734-8_4.

[27] M. Hakkarainen, S. Karlsson, A.-C. Albertsson, Rapid (bio)degradation of polylactide by mixed culture of compost microorganisms—low molecular weight products and matrix changes, Polymer 41 (2000) 2331–2338, https://doi.org/10.1016/S0032-3861(99)00393-6.

[28] N.B. Erdal, M. Hakkarainen, Degradation of cellulose derivatives in laboratory, man-made, and natural environments, Biomacromolecules 23 (2022) 2713–2729, https://doi.org/10.1021/acs.biomac.2c00336.

[29] N. Yadav, M. Hakkarainen, Degradable or not? cellulose acetate as a model for complicated interplay between structure, environment and degradation, Chemosphere 265 (2021) 128731, https://doi.org/10.1016/j.chemosphere.2020.128731.

[30] P. Baruah, R. Duarah, N. Karak, Tannic acid-based tough hyperbranched epoxy thermoset as an advanced environmentally sustainable high-performing material Iran, Polym. J. 25 (2016) 849–861, https://doi.org/10.1007/s13726-016-0471-3.

[31] W.S. Chow, S.G. Tan, Z. Ahmad, et al., Biodegradability of epoxidized soybean oil based thermosets in compost soil environment, J. Polym. Environ. 22 (2014) 140–147, https://doi.org/10.1007/s10924-013-0615-x.

[32] J. Chen, H. Liu, W. Zhang, L. Lv, Z. Liu, Thermosets resins prepared from soybean oil and lignin derivatives with high biocontent, superior thermal properties, and biodegradability, J. Appl. Polym. Sci. 137 (2020) 26, https://doi.org/10.1002/APP.48827.

[33] G. Foli, M. Degli Esposti, D. Morselli, P. Fabbri, Two-step solvent-free synthesis of poly(hydroxybutyrate)-based photocurable resin with potential application in stereolithography, Macromol. Rapid Commun. 41 (2020) 1900660, https://doi.org/10.1002/marc.201900660.

[34] J. Yao, M. Morsali, A. Moreno, M.H. Sipponen, M. Hakkarainen, Lignin nanoparticle-enhanced biobased resins for digital light processing 3D printing: towards high resolution and tunable mechanical properties, Eur. Polym. J. 194 (2023) 112146, https://doi.org/10.1016/j.eurpolymj.2023.112146.

[35] J. Yao, M. Hakkarainen, Methacrylated wood flour-reinforced “all-wood” derived resin for digital light processing (DLP) 3D printing, Comp. Comm. 38 (2023) 101506, https://doi.org/10.1016/j.coco.2023.101506.

[36] J. Yao, M. Karlsson, M. Lawoko, K. Odelius, M. Hakkarainen, Microwave-assisted organosolv extraction for more native-like lignin and its application as a property enhancing filler in a light processable biobased resin, RSC Sustainability 1 (2023) 1211–1222, https://doi.org/10.1039/D3SU00115F.

[37] N.K. Kalita, M. Hakkarainen, Triggering degradation of cellulose acetate by embedded enzymes: accelerated enzymatic degradation and biodegradation under simulated composting conditions, Biomacromolecules 24 (2023) 3290–3303, https://doi.org/10.1021/acs.biomac.3c00337.

[38] G.E. Yu, R.H. Marchessault, Characterization of low molecular weight poly (β-hydroxybutyrate)s from alkaline and acid hydrolysis, Polymer 41 (2000) 1087–1098, https://doi.org/10.1016/S0032-3861(99)00230-X.

[39] S. Oprea, S. Vlad, A. Stanciu, Poly(urethane-methacrylate)s Synthesis and Characterization, Polymer 42 (2001) 7257–7266, https://doi.org/10.1016/S0032-3861(01)00206-3.

[40] Y. Zhang, Y. Li, L. Wang, Z. Gao, M.R. Kessler, Synthesis and Characterization of Methacrylated Eugenol as a Sustainable Reactive Diluent for a Maleinated Acrylated Epoxidized Soybean Oil Resin, ACS Sustain. Chem. Eng. 5 (2017) 8876–8883, https://doi.org/10.1021/acssuschemeng.7b01673.

[41] M. Maturi, C. Pulignani, E. Locatelli, V. Vetri Buratti, S. Tortorella, L. Sambri, M. Franchini Comes, Phosphorescent bio-based resin for digital light processing (DLP) 3D-printing, Green Chem. 22 (2020) 6212–6224, https://doi.org/10.1039/D0GC01983F.

[42] A. Hou, C. Zhang, Y. Wang, Preparation and UV-protective properties of functional cellulose fabrics based on reactive azobenzene Schiff base derivative, Carbohydr. Polym. 87 (2012) 284–288, https://doi.org/10.1016/j.carbpol.2011.07.055.

[43] S. El-Sayed Saeed, T.M. Al-Harbi, M.S.A. Abdel-Mottaleb, A.N. Al-Hakimi, A.E.A. E. Albadria, M.M.A. El-Hady, Novel Schiff base transition metal complexes for imparting UV protecting and antibacterial cellulose fabric: Experimental and

computational investigations, Appl. Organomet. Chem. 36 (2022) 12, https://doi.org/10.1002/aoc.6889.
[44] R. Erwin Abdul, S. Fumio, M. Toshio, Synthesis and properties of a novel polyacetylene containing eugenol moieties, J. Macromol. Sci., Part a: Pure Appl. Chem. A 41 (2004) 133–141, https://doi.org/10.1081/MA-120027299.
[45] L. Rojo, J.M. Barcenilla, B. Vázquez, R. González, San Román, J. Intrinsically Antibacterial Materials Based on Polymeric Derivatives of Eugenol for Biomedical Applications, Biomacromolecules 9 (2008) 2530–2535, https://doi.org/10.1021/bm800570u.
[46] A. Liguori, H. Xu, D. Hazarika, M. Hakkarainen, Simple Non-Equilibrium atmospheric plasma post-treatment strategy for surface coating of digital light processed 3D-printed vanillin-based schiff-base thermosets, ACS Appl. Polym. Mater. 5 (2023) 8506–8517, https://doi.org/10.1021/acsapm.3c01632.
[47] J.F. Stanzione III, J.M. Sadler, J.H. La Scala, R.P. Wool, Lignin model compounds as bio-based reactive diluents for liquid molding resins, ChemSusChem 5 (2012) 1291–1297, https://doi.org/10.1002/cssc.201100687.
[48] C. Zhang, S.A. Madbouly, M.R. Kessler, Renewable polymers prepared from vanillin and its derivatives, Macromol. Chem. Phys. 216 (2015) 1816–1822, https://doi.org/10.1002/macp.201500194.
[49] T. Ma, R. Wang, S. Jin, S. Zheng, L. Li, J. Shi, Y. Cai, J. Liang, Z. Tao, Functionalized boron nitride-based modification layer as ion regulator toward stable lithium anode at high current densities, ACS Appl. Mater. Interfaces 1 (2019) 2535–2542, https://doi.org/10.1021/acsami.0c16354.
[50] M. Delahaye, J.M. Winne, F.E. Du Prez, Internal catalysis in covalent adaptable networks: phthalate monoester transesterification as a versatile dynamic cross-linking chemistry, J. Am. Chem. Soc. 141 (2019) 15277–15287, https://doi.org/10.1021/jacs.9b07269.
[51] J.H. Chen, X.P. An, Y.D. Li, et al., Reprocessible epoxy networks with tunable physical properties: synthesis, stress relaxation and recyclability, Chin. J. Polym. Sci. 36 (2018) 641–648, https://doi.org/10.1007/s10118-018-2027-9.
[52] K. Yu, P. Taynton, P. Zhang, M.L. Dunn, J.H. Qi, Reprocessing and recycling of thermosetting polymers based on bond exchange reactions, RSC Adv. 4 (2014) 10108–10117, https://doi.org/10.1039/C3RA47438K.
[53] L. Lu, J. Pan, G.J. Li, Recyclable high-performance epoxy based on transesterification reaction, Mater. Chem. A 5 (2017) 21505–21513, https://doi.org/10.1039/C7TA06397K.
[54] P. Flory, Principles of Polymer Chemistry, Cornell University Press, 1953.
[55] S. Basak, J.C.M. Angel, K.A. Cavicchi, Thermal annealing of high cis-1,4-polybutadiene/octadecyl acrylate blends as a one-step process for fabricating shape memory polymers, ACS Appl. Polym. Mater. 5 (2023) 1585–1595, https://doi.org/10.1021/acsapm.3c00319.
[56] T. Katoh, Y. Ogawa, Y. Ohta, T. Yokozawa, Synthesis of polyester by means of polycondensation of diol ester and dicarboxylic acid ester through ester–ester exchange reaction, J. Polym. Sci. 59 (2021) 787–797, https://doi.org/10.1002/pol.20210032.
[57] A. Liguori, E. Oliva, M. Sangermano, M. Hakkarainen, Digital light processing 3D printing of isosorbide- and vanillin-based ester and ester-imine thermosets: structure-property recyclability relationships, ACS Sustain. Chem. Eng. 11 (2023) 14601–14613, https://doi.org/10.1021/acssuschemeng.3c04362.
[58] X. Yang, J. Clénet, H. Xu, K. Odelius, M. Hakkarainen, Two step extrusion process: from thermal recycling of PHB to plasticized PLA by reactive extrusion grafting of PHB degradation products onto PLA chains, Macromolecules 48 (2015) 2509–2518, https://doi.org/10.1021/acs.macromol.5b00235.
[59] N.B. Erdal, K.H. Adolfsson, T. Pettersson, M. Hakkarainen, Green strategy to reduced nanographene oxide through microwave assisted transformation of cellulose, ACS Sustain. Chem. Eng. 2 (2014) 2198–2203, https://doi.org/10.1021/acssuschemeng.7b03566.
[60] J. Xu, B.H. Guo, R. Yang, Q. Wu, G.Q. Chen, Z.M. Zhang, In situ FTIR study on melting and crystallization of polyhydroxyalkanoates, Polymer 43 (2002) 6893–6899, https://doi.org/10.1016/S0032-3861(02)00615-8.
[61] Y. Kann, M. Shurgalin, R.K. Krishnaswamy, FTIR spectroscopy for analysis of crystallinity of poly(3-hydroxybutyrate-co-4 -hydroxybutyrate) polymers and its utilization in evaluation of aging, orientation and composition, Polym. Test. 40 (2014) 218–224, https://doi.org/10.1016/j.polymertesting.2014.09.009.
[62] A. Bher, Y. Cho, R. Auras, Boosting degradation of biodegradable polymers, Macromol. Rapid Commun. 44 (2003) 2200769, https://doi.org/10.1002/marc.202200769.
[63] S. Subramaniyan, N. Najjarzadeh, S.R. Vanga, A. Liguori, P.O. Syrén, M. Hakkarainen, Designed for circularity: chemically recyclable and enzymatically degradable biorenewable Schiff-base polyester-imines, ACS Sustain. Chem. Eng. 11 (2023) 3451–3465, https://doi.org/10.1021/acssuschemeng.2c06935.